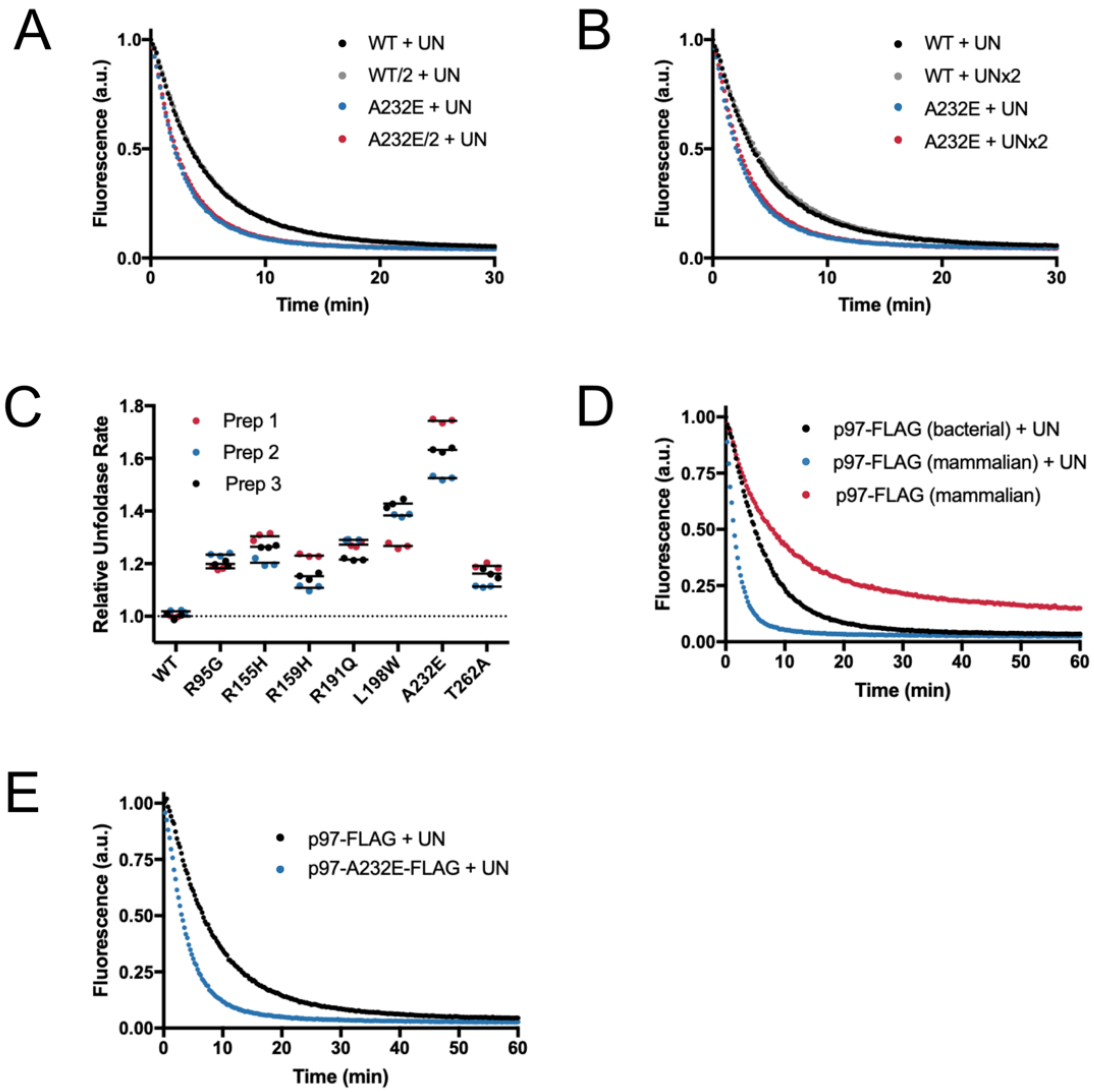

Figure S1. Related to Figure 1. (A) Example time courses of unfolding of split mEos3.2 show little change in normalized rate when the concentration of p97 is halved (WT: 0.985 ± 0.005, p97-A232E: 0.937 ± 0.006). **(B)** Example time courses show little change in normalized rate when UN is doubled (WT: 0.927 ± 0.002, p97-A232E: 0.93 ± 0.01). **(C)** Prep-to-prep variability in the unfoldase rates of MSP-mutant p97. All MSP mutants showed increased unfoldase rates compared to wild type yet with considerable prep-to-prep variabilities. For Preps 1 and 2, assays were carried out in a modified assay buffer under slightly different conditions (see Methods), and substrate-unfoldase rates were normalized to that of wild-type p97 Prep 1. The rates for the Prep 3 are replotted from Figure 1C. **(D)** Example mEos3.2 substrate-unfolding traces show that human cell-line expressed p97 in complex with UN (blue trace) is a faster unfoldase than *E. coli*-expressed p97·UN (black trace) and can promote unfolding even without the addition of exogenous UN (red trace). **(E)** Example unfolding traces show human cell-line expressed p97-A232E unfolds substrate faster than similarly expressed wild-type p97. Representative traces shown. Technical replicates, n ≥ 2, ± S.D..

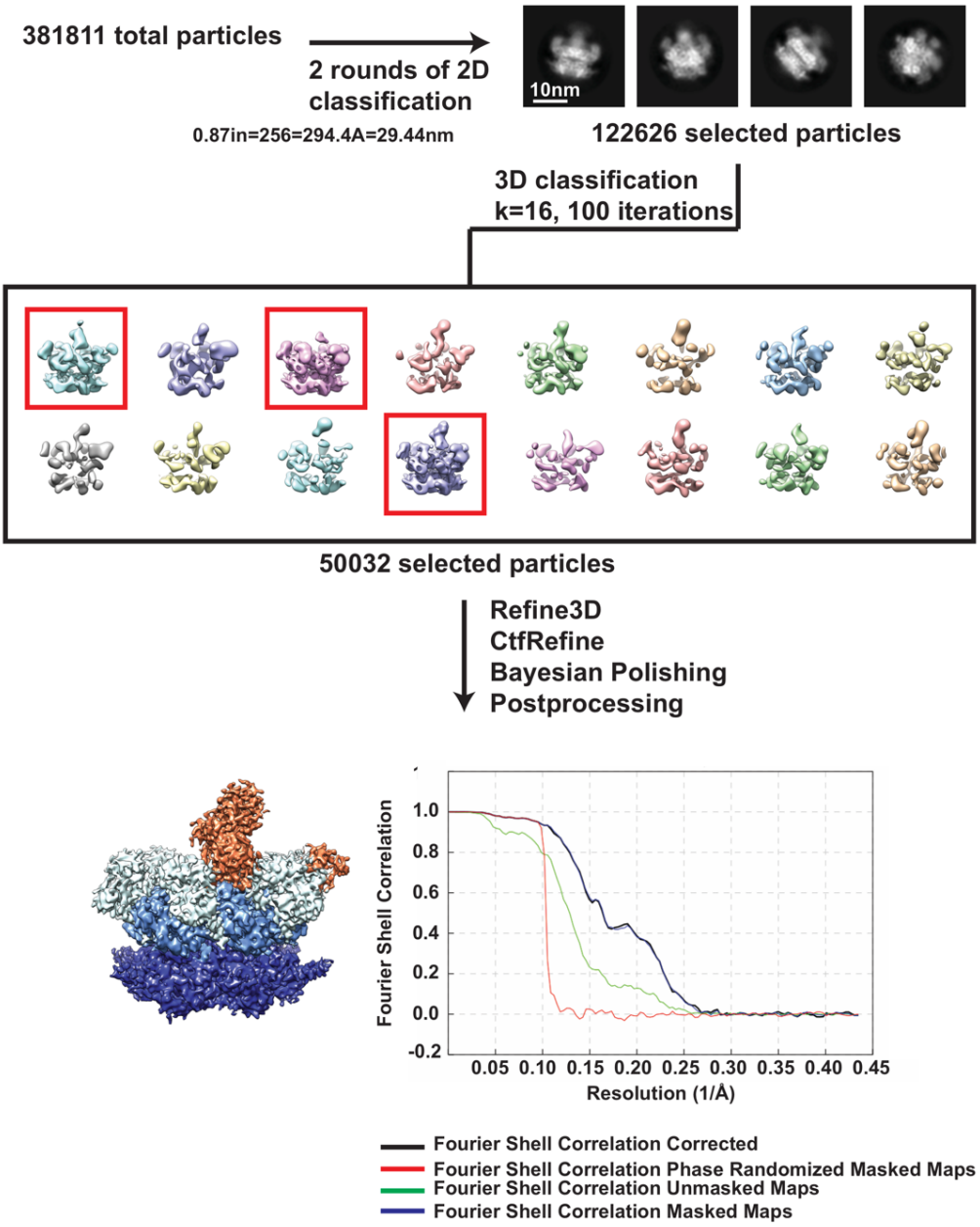

Figure S2. Related to Figure 3. Analysis and cryo-EM processing of the p97-A232E:UN-ATP complex. Total particles of p97-A232E:UN-ATP complex dataset were subjected to two rounds of reference-free 2D class averages to clean out contamination or bad particles, followed by a 3D classification into 16 classes. The three best classes of particles were selected from the total 16 classes (red box), resulting in a final dataset of 50,032 particles. This particle stack was refined with CtfRefinement, Bayesian polishing, and post-processing, resulting in a final resolution of 4.26Å, evaluated using gold standard FSC curves of the masked and unmasked post-processed final reconstructions (Scheres, 2012). The final map is colored by domains: NPLOC4 (orange), NTDs (light blue), D1 (sky blue), D2 (navy blue).

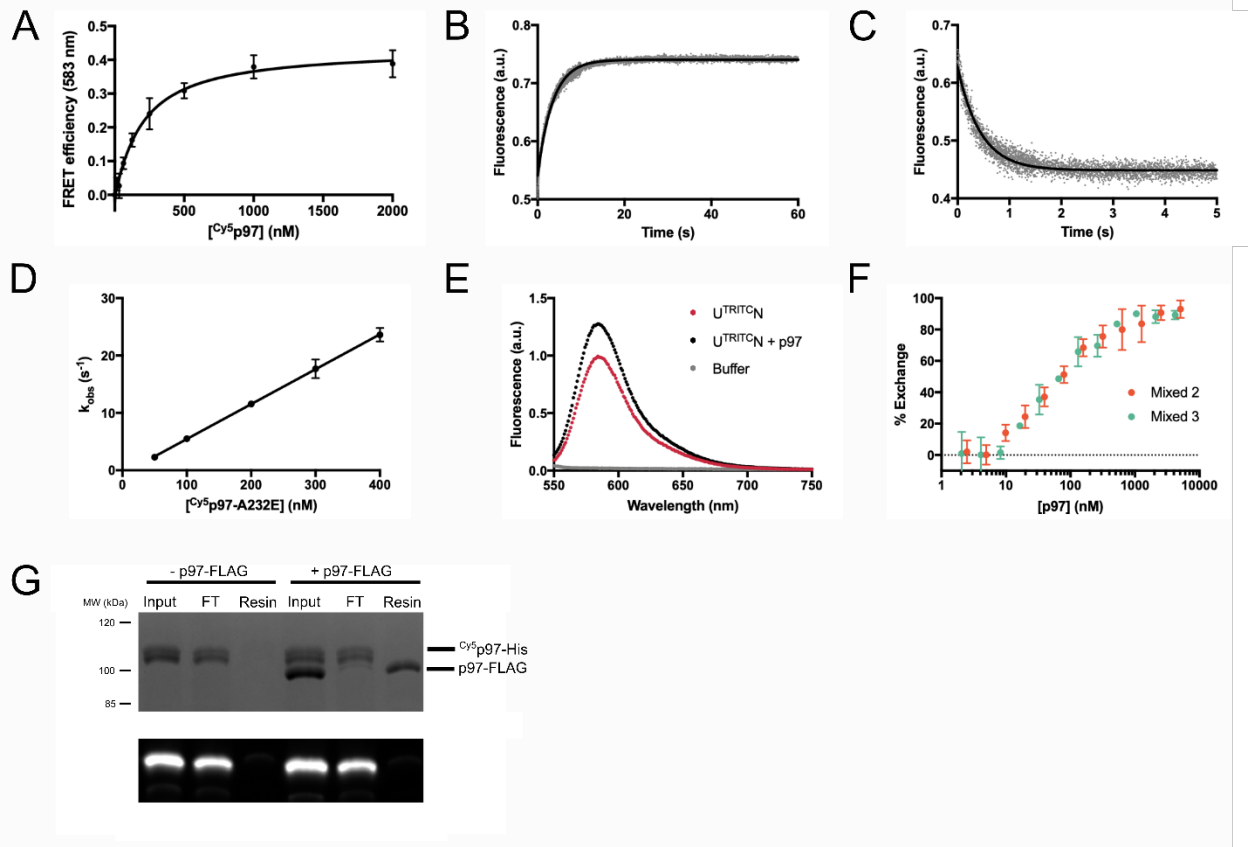

Figure S3. Related to Figure 5 and Table 1. (A) Example FRET-based binding curve for the interaction of $U^{TRITC}N$ with variable concentrations of $^{Cy5}p97$ in ATPγS. Data were fit to a quadratic binding equation (technical replicates, N = 3, ± S.D.). **(B)** Example trace and single-exponential fit for the dissociation of $U^{TRITC}N$ from $^{Cy5}p97$ in ATPγS, measured by the recovery of donor TRITC fluorescence after stopped-flow mixing. **(C)** Example trace and single-exponential fit for the binding of $U^{TRITC}N$ to $^{Cy5}p97$ in ATPγS, measured by the quenching of donor TRITC fluorescence after stopped-flow mixing. **(D)** Shown are the observed rate constants k_{obs} for the association of $U^{TRITC}N$ with $^{Cy5}p97$-A232E in ATPγS, derived from single-exponential fits of binding kinetics at various $^{Cy5}p97$-A232E concentrations. The association rate constant, k_{on}, was determined by linear regression (technical replicates, N ≥ 5, ± S.D.). **(E)** $U^{TRITC}N$ fluorescence (red, 50 nM) is sensitive to binding of unlabeled p97 (black, 2.5 μM). (**F**) Competition FRET experiment, monitoring the dissociation of $U^{TRITC}N$ from Cy5-labeled p97-A232E and binding to excess unlabeled Mixed 2 and Mixed 3 heterohexamers, show that the mixed heterohexamers have similar UN affinities (technical replicates, N ≥ 2, ± S.D.). **(G)** Protomer exchange between p97 hexamers is slow. Coomassie stain and fluorescence scan of an SDS-PAGE gel show no evidence of His-tagged $^{Cy5}p97$ binding to the anti-FLAG resin despite robust binding of FLAG-tagged p97.

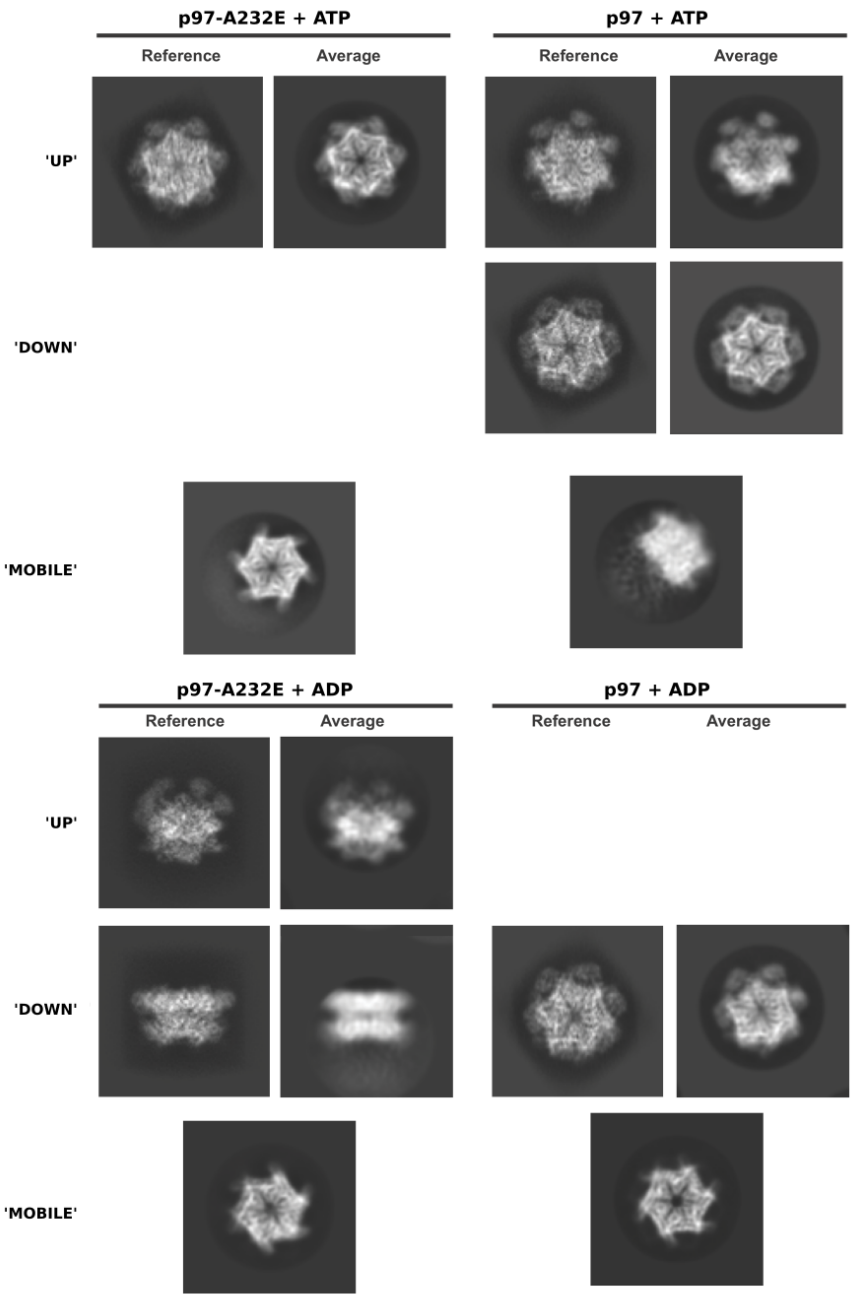

Figure S4: Related to Figure 6. Representative 2D class averages of nucleotide datasets, compared to back projections of 3D models. Back projections of the 3D models for p97-ATPγS (EMD:3297) and p97-ADP (EMD:3299) (Banerjee et al., 2016) next to a representative 2D class average from each nucleotide dataset, oriented in the same angle. Representative averages are also shown for hexamers with ‘mobile’ NTDs.

	p97-A232E-UN:ATP	p97-ATP	p97-A232E-ATP	p97-ADP	p97-A232E-ADP
Microscope	Titan Krios	Talos Arctica			
Nominal Mag.	33,333x	43,860x			
Detector	K2			K3	
Pixel Size (Å/pixel)	1.15	1.16		1.14	
Exposure (s)	8			5.273	
Frame rate (s)	0.2			0.12	
Total electron dose	48				
Defocus Range (μm)	-1 to -2.5				
Total Micrographs	5897	1100	704	706	1781
Total Particles	164673	170204	141281	414495	181424

Table S1. Related to Figure 3 and Figure 6. Parameters for the cryo-EM data collection.